Injection Seeding of a Q-switched Nd:YLF Oscillator

by

Gary Ball

Submitted in Partial Fulfillment

of the

Requirements for the Degree

MASTER OF SCIENCE

Supervised by

Dr. Wolf Seka

Department of Optics

College of Engineering and Applied Science

University of Rochester

Rochester, New York

1987

Acknowledgments

Abstract

This dissertation presents a study of injection seeding in Nd:YLF Q-switched oscillators for the purposes of producing single axial mode output. The objective was to develop a prototype system and determine the limiting factors which dictate successful injection seeding. The laser system consisted of a laser diode pumped monolithic miniature Nd:YLF master oscillator which seeded a conventional Q-switched Nd:YLF slave oscillator. The limiting factor of our present system was determined to be spatial hole burning for which preventative alternatives are suggested. The analysis of our present laser system has permitted us to draw conclusions concerning the optimal injection seeding of a monomode Q-switched laser.

Table of Contents

Appendices

List of Figures

I. Introduction

In the future, pulse shaping in the one to several nano-second regime is likely to be important for high density/high yield laser fusion experiments. In order to generate such pulses a reliable monomode Q-switched oscillator will be needed. Injection seeding is a promising way of achieving this as high gain and short transient buildup times make interferometric mode selection more difficult. The basic concept relies on a small, well controlled single mode oscillator whose output is injected into a mode-matched, stable or unstable, oscillator to produce a single-mode Q-switched pulse with desired spatial and temporal characteristics. The goal of this dissertation is to develop a detailed understanding of injection seeding and the operating constraints of such a laser system.

The system under study is not a novel one, but a reapplication and study of previously designed injection seeding systems for spectroscopic applications. To date, injection seeding has been typically applied to Nd:YAG and gas laser systems. One goal of this paper is to determine differences in Nd:YAG and Nd:YLF seeding systems. In 1981 Park [1 and 2] reported on frequency and mode control of a Q-switched Nd:YAG laser by injection seeding. This study utilized two relatively high power Q-switched oscillators, one being well controlled, and observed the effects which the well controlled oscillator had on the second oscillator. This work was followed by the development of a series of small, well controlled monolithic lasers utilizing laser diodes as narrow band end pumping devices [3-6]. In 1986 Schmitt and Rahn [7] designed and tested a compact injection seeding system which permitted highly reliable single-axial-mode operation of a Q-switched Nd:YAG laser over periods of hours.

In this dissertation a laser-diode-pumped Nd:YLF laser injection seeding system will be studied. The design will follow that of Schmitt and Rahn. Frequency stability per se is not important but monomode output is.

II. Theory

The use of a weak monochromatic signal to control the frequency and temporal characteristics of a free running oscillator may be separated into two regimes: the steady state, injection locking, and the transient, injection seeding. In the steady state regime (CW operation) the monochromatic output of a small weak well controlled oscillator, the master oscillator, is injected into a second free running higher power oscillator, the slave oscillator. If the injected signal is of sufficient magnitude and has its frequency within the "injection locking range," the injected signal will dominate the emission of the slave oscillator causing it to oscillate at the injected frequency rather than its eigenfrequency. This technique is referred to as injection locking.

Injection seeding, on the other hand, pertaining to pulsed lasers, works in the transient regime. In this case, the weak monochromatic signal from the master oscillator is used to define the initial conditions which dictate the buildup of the photon flux in the slave oscillator. Injected signals which are high enough above the fluorescence noise level of the slave oscillator will seed the nearest eigenmode of the slave oscillator and saturate the gain medium well before the other modes, driving the slave oscillator to lase on a single axial eigenmode.

II.1. Theoretical Model

Injection seeding of high power lasers was thoroughly treated by Y.K.Park *et al.* [8] and Jean-Louis Lechambre *et al.* [9]. Rather than repeating their analytical model, this dissertation will closely follow Siegman's[10] "Pulsed Injection Locking: A Phasor Description." Siegman uses a phasor description to describe the evolution of the injection seeded pulse, utilizing the linear superposition of electric fields. It is both elegant and effective in illustrating injection seeding concepts.
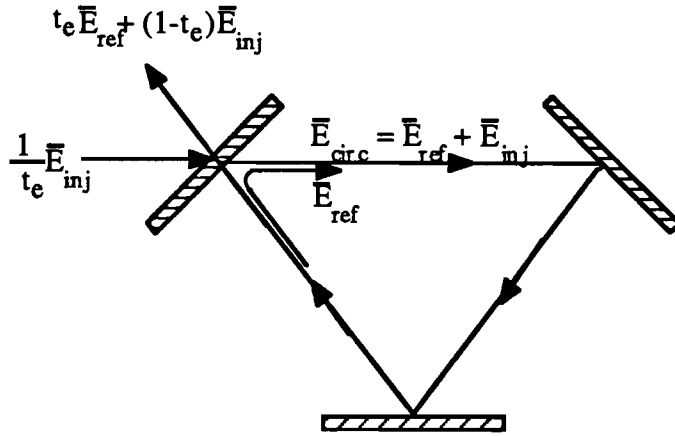
Fig. 1: Model of a ring oscillator (t_e= amplitude transmission of injection mirror).

Fig. 1 illustrates the evolution of the electric field vectors (phasors) inside a ring oscillator, where $\overline{E}_{circ}$ is the total phasor amplitude of the circulating electric field in the optical cavity, $\overline{E}_{ref}$ is the portion of the circulating field which is reflected by the injection mirror, and $\overline{E}_{inj}$ is the injected field inside the cavity (t_e is the amplitude transmission of the injection mirror). While Fig. 1 refers to a ring cavity, the model equally applies to any other cavity configuration with injection at any point within the cavity (e.g. end mirror, polarizer, etc).

At the beginning of each new round trip the circulating field is given by

$$\overline{E}_{circ}(t) = \overline{E}_{ref}(t) + \overline{E}_{inj}(t) \ . \tag{1}$$

The phasor diagrams (Figs. 2 and 3) are defined with respect to the frequency, ω_1, of the injected signal such that the phasors do not appear to rotate in this diagram if their frequency is ω_1. Note that the eigenfrequency of the slave oscillator is ω_0 which obeys the relationship $\omega_0 T = n2\pi$, where T is the slave cavity round trip time and n is an integer. (ω_0 is not necessarily equal to ω_1.) All three complex phasor amplitudes may be time varying within the slowly varying envelope approximation.

After one round trip the electric field reflected by the injection mirror is

$$\bar{E}_{ref}(t) = \bar{E}_{circ}(t-T)e^{\delta_m - \delta_c - jT(\omega_1 - \omega_0)} , \qquad (2)$$

which reflects the gain, e^{δ_m}, the losses, $e^{-\delta_c}$, and the residual phase angle $\phi=(\omega_1-\omega_0)T$ due to the difference between the injected frequency ω_1 and the oscillator eigenfrequency ω_0. The quantities δ_m and δ_c are the amplitude gain and loss coefficients for one round trip. In terms of power transmission and reflectivities we find $R_1 R_2 L = e^{-2\delta_c}$ where L accounts for any additional cavity losses.

Equations (1) and (2) provide a good description of the evolution of the laser oscillation inside a resonator provided the magnitudes of $\bar{E}$, δ_m, and δ_c do not vary too much over one round trip transit time. If they do, average values of δ_m and δ_c should be used. From Eqs. (1) and (2) a recursive formula (Eq. 3) for the buildup of the electric field inside the resonator can be obtained,

$$\bar{E}_{circ}(t) = \bar{E}_{circ}(t-T)e^{\delta_m - \delta_c - jT(\omega_1 - \omega_0)} + \bar{E}_{inj}(t). \qquad (3)$$

This equation forms the basis for our analysis of injection locking and injection seeding of a slave oscillator.

II.2. Steady State Regime

In the steady state regime we can distinguish two cases; above and below threshold operation. Fig. 2 illustrates the phasor diagram below threshold. In this case , $\bar{E}_{circ}$ returns after one round trip as $\bar{E}_{ref}$ which is smaller in magnitude and out of phase by

$\Delta\omega T = T(\omega_1 - \omega_0)$ from $\overline{E}_{circ}$ of the previous round trip. $\overline{E}_{inj}$ then adds with $\overline{E}_{ref}$ to reset the phase and amplitude of $\overline{E}_{circ}$ to its steady state magnitude and direction.

$$\overline{E}_{circ} = \overline{E}_{ref} + \overline{E}_{inj}$$
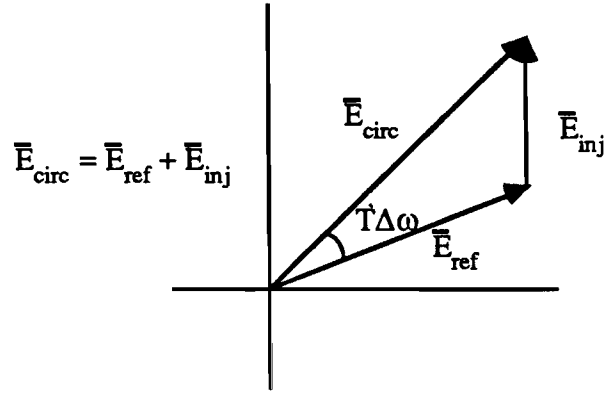
Figure 2: Phasor diagram for steady state operation below threshold.

Solving Eq. (3) in the steady state regime leads to the following equation:

$$\overline{E}_{circ} = \frac{\overline{E}_{inj}}{1 - \exp[\delta_m - \delta_c - jT(\omega_1 - \omega_0)]} \, . \tag{4}$$

Above threshold (Fig. 3) the cavity runs at its free running oscillation level with a gain of unity. Since we are only interested in a system which produces a significantly larger signal than that with which it was seeded, $|\overline{E}_{circ}| \approx |\overline{E}_{ref}| >> |\overline{E}_{inj}|$, we find the maximum

$$\overline{E}_{circ} = \overline{E}_{ref} + \overline{E}_{inj}$$
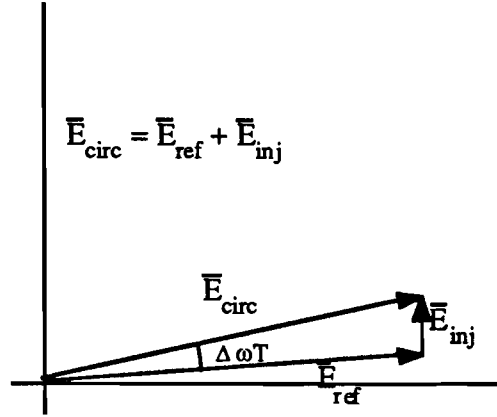
Figure 3: Phasor diagram for steady state operation above threshold.

detuning angle, $\pm\omega_m$, to occur when $\overline{E}_{circ}$ and $\overline{E}_{inj}$ are out of phase by $\approx 90°$. In this case the detuning angle is given by

$$|T(\omega_1 - \omega_0)| \le T\omega_m \approx \left|\frac{\overline{E}_{inj}}{\overline{E}_{circ}}\right| \quad . \tag{5}$$

This leads to a half-injection-locking-range of

$$\omega_m = \frac{1}{T}\sqrt{\frac{I_{inj}}{I_{circ}}} \tag{6}$$

where the electric fields were converted to the appropriate intensities $I_{inj}\alpha|\overline{E}_{inj}|^2$ and $I_{circ}\alpha|\overline{E}_{circ}|^2$. It is important to note that $\overline{E}_{circ}$ appears stationary in the phasor diagram indicating that its frequency is that of the injected signal. Because I_{inj} is typically very small compared to I_{circ} the injection locking range is quite small. (Note I_{circ} and I_{inj} are both measured inside the cavity.)

II.3. Transient Regime

In high gain Q-switched lasers the steady state locking regime is not reached as the injected signal is no longer able to close the gap between the reflected signal and the circulating signal. We assume that for times t<0 the gain and losses are below threshold, and for times t≥0 the losses are reduced so that an overall gain above threshold is obtained. We further assume a constant $\bar{E}_{inj}$ and an instantaneous Q-switch at t=0. This model is not limited by these assumptions, but applies equally well to a Q-switch with finite turn on time and a variable injection intensity. This will be discussed in more detail later.
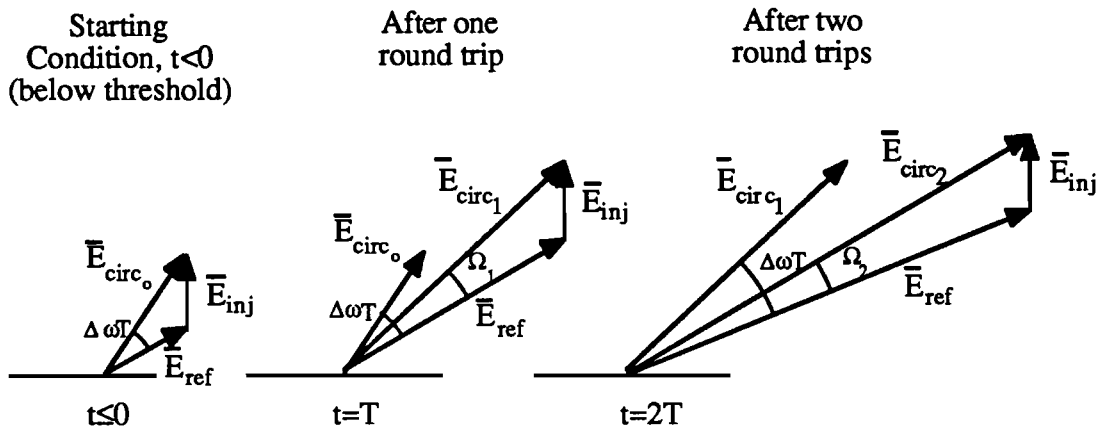
Figure 4: Phasor evolution on successive round trips during buildup of laser oscillation.

If the injected signal has been turned on for a few round trip times previous to t=0 the starting condition (below threshold) is defined by the steady state condition, Eq. (4). At time t=0 the cavity losses are lowered and the circulating electric field inside the cavity is amplified. After one round trip, $\bar{E}_{ref}(T)$ returns larger in magnitude from $\bar{E}_{circ}(0)$ and rotated by $\phi=(\omega_1-\omega_0)T$. $\bar{E}_{inj}$ is then added to $\bar{E}_{ref}$, summing the vectors to $\bar{E}_{circ}(T)$ which is both larger than $\bar{E}_{circ}(0)$ and out of phase by $(\Delta\omega T- \Omega_1)$. After two round trips $\bar{E}_{ref}(2T)$ has grown still larger and after the addition of the injected field the new circulating field $\bar{E}_{circ}(2T)$ is out of phase from $\bar{E}_{circ}(T)$ by $(\Delta\omega T- \Omega_2)$.

Since $\bar{E}_{ref}$ grows exponentially on each round trip, the magnitude of $\bar{E}_{inj}$ soon becomes negligible compared to $\bar{E}_{ref}$ and Ω goes to zero. Thus, on each round trip $\bar{E}_{ref}$ rotates by an angle ϕ relative to the preceding $\bar{E}_{circ}$ resulting in a linearly increasing phase factor,

$$\phi(t) \approx -(\omega_1 - \omega_2)T \times (t/T) = -(\omega_1 - \omega_0)t \quad . \tag{7}$$

The actual frequency, ω, of the electric field inside the cavity is then,

$$\omega(t) = \omega_1 + \frac{\partial \phi(t)}{\partial t} = \omega_0 , \tag{8}$$

i.e. the injected frequency has shifted onto the cavity resonance frequency.

An exact measurement of how the frequency is shifted from ω_1 to ω_0 cannot be made since the time intervals of interest (round trip time) limit spectral resolution by the uncertainty principle $\Delta v \Delta t \approx 1$. For example, if the frequency measurement is made within one round trip, the spectrum may only be measured with an accuracy of roughly one free spectral range.

III. Mode Selection in a Q-Switched Oscillator

III.1. Q-switched Pulse Buildup

The pulse intensity buildup in a Q-switched oscillator along with the gain coefficient and cavity losses are illustrated in Fig. 5. We note that while the signal is small the intensity grows linearly on the logarithmic scale. Once the signal grows to a size where it depletes a significant portion of the stored energy during each round trip the intensity follows a nonlinear path to its peak. At the peak of the pulse the gain coefficient goes through its threshold value and the pulse decays through cavity losses.
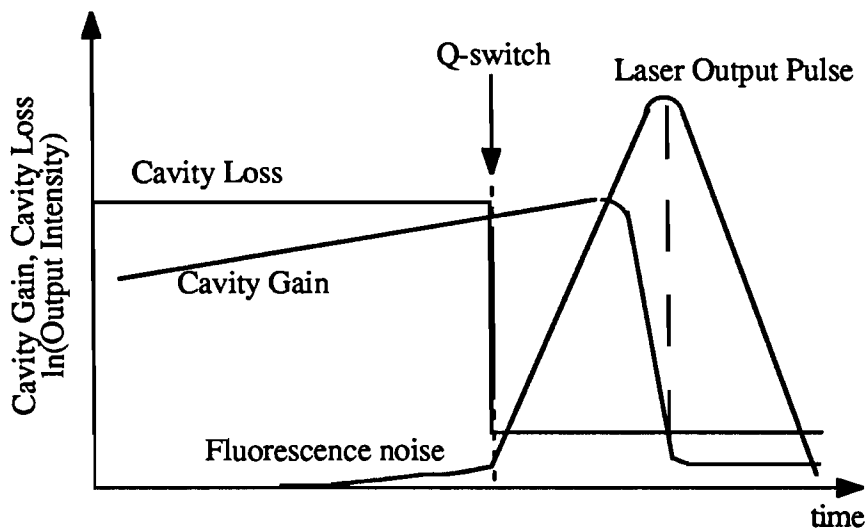
Figure 5: Schematic evolution of the pulse buildup intensity, gain coefficient, and cavity losses in a Q-switched oscillator.

Q-switched oscillators typically exhibit multimode output because of short pulse buildup times and large gain bandwidths compared to the cavity free spectral range. The modes that lase essentially have the same gain resulting in negligible cavity discrimination.

Since on the whole, the modes share the same part of the gain medium, they grow at the same rate until they saturate the gain causing all the modes to peak at the same time. The various oscillating modes generally have statistically distributed amplitudes and relative phases, and all of them contribute to a more or less smooth and reproducible output pulse. The total energy contained in the pulse is the sum of the individual modes.

By contrast, mode selection via injection seeding is conceptually illustrated in Fig. 6. A monochromatic signal, from a master oscillator, is injected into a Q-switched oscillator. If the signal is injected off resonance, the frequency of the injected pulse will switch onto resonance after a few round trips as described in the previous section. If, at that time the injected signal is still significantly above the noise signal, i.e. the sum of the intensities of all modes having maximum gain, the injected signal will dominate the output of the oscillator as shown in Fig. 6. Thus the buildup time of the injection seeded pulse is shorter than that of the free running Q-switched oscillator which had to start up from noise.
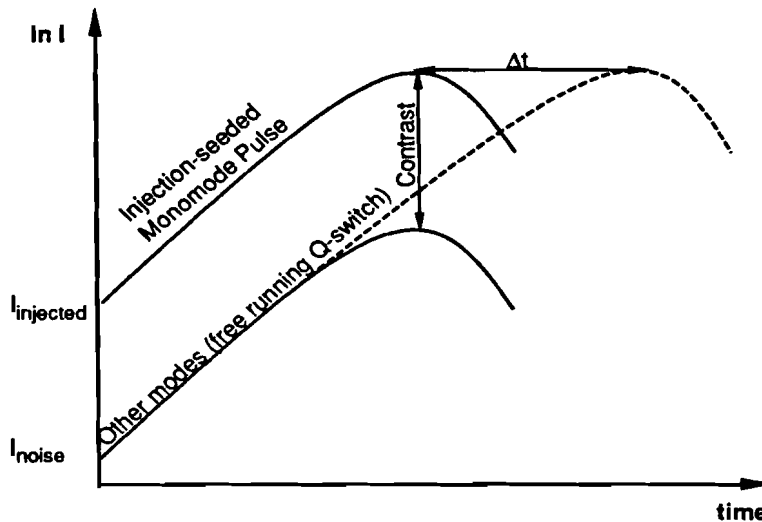
Figure 6: Injected signal buildup and noise signal buildup.

If we assume that the injection-seeded monomode pulse saturates the entire gain medium (e.g. traveling wave oscillator) then all of the modes which spontaneously grow out of the fluorescence noise will saturate at the same time as the monomode pulse. Consequently, if the injected signal is sufficiently high above the fluorescence noise (or amplified spontaneous emission) a monomode pulse will appear if all other oscillating modes together have much lower intensities.

Returning to the evolution of $\overline{E}_{circ}$ during the first few round trips after the cavity losses are switched, we can solve Eq. (3) iteratively, on each round trip, to give a plot such as shown schematically in Fig. 7. After a few round trips the curves for the different detuning angles all exhibit equal slopes but are displaced along the time (or intensity) axis; the further off-resonance the injected signal is the larger the displacement.It is then the
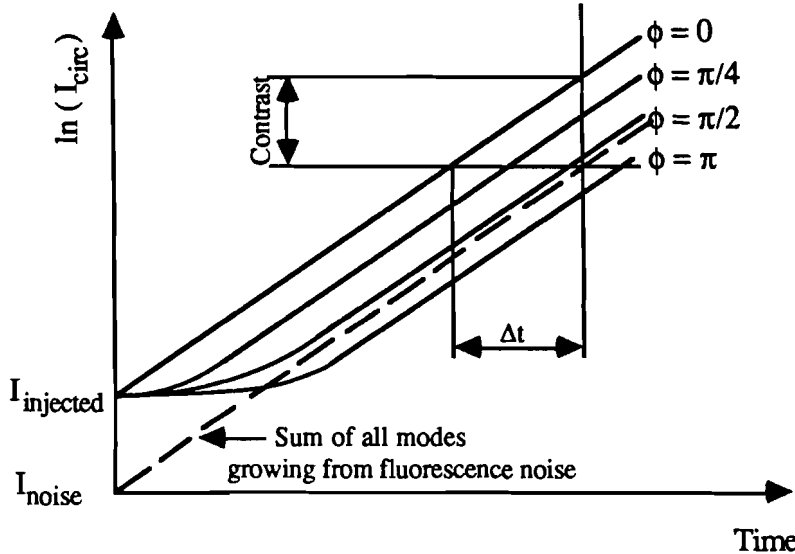
Figure 7: Schematic evolution of injection-seeded pulse for various detuning angles $\phi=(\omega_1-\omega_0)T$.

contrast (difference in intensity) between the injected signal after its growth has stabilized and the amplified noise signal at that time, which will result in the final contrast between the

injection-seeded pulse and the free-running Q-switch pulse. If the contrast is large enough, the resultant output will appear monomode.

This contrast can be converted to pulse buildup time. This relation is also illustrated in Fig. 7. Experimentally, it is much easier to quantify a change in buildup time than a change in contrast. These relationships will be further discussed later.

III.2. Amplified Spontaneous Emission (ASE)

The objective of injection seeding is to start one longitudinal mode above the noise level causing it to reach saturation before the other modes. ASE is the source of the noise with which the seeded signal has to compete. ASE is mostly due to spontaneous emission from a small region at either end of the laser rod. This emission will then be amplified by the small signal gain over the full length of the rod. The ASE may be further increased by reflection at the output coupler of a linear resonator and a second pass through the rod if the single pass gain is greater than the losses at the output coupler.

For a linear cavity the ASE intensity[11] may be written as

$$I_{ASE} = \frac{\gamma_{rad}\hbar\omega a^2}{4\sigma L^2} G_0 \times (1 + R G_0) \quad , \tag{9}$$

where we assumed a large single pass power gain, G_0, of the active medium. Also, R is the reflectivity of the output coupler, σ is the stimulated emission cross section, and γ_{rad} is the radiative decay rate. The $(a/L)^2$ term is related to the solid angle of the transverse mode oscillating in the resonator and may be approximated by $(w_0/L)^2$ where w_0 is the gaussian beam waist and L is the cavity length. The beam waist [12] is given by

-12-

$$\frac{\pi n w_o^2}{\lambda} = (LR_2)^{1/2}(1-\frac{L}{R_2})^{1/2} \quad , \tag{10}$$

where R_2 is the radius of curvature of the back mirror of the cavity of a half-symmetric (hemispherical) resonator and n is the index of refraction.

I_{ASE} is the total ASE intensity in the fundamental transverse mode within the cavity. As discussed in Sec. III.1, several axial modes will lase due to negligible gain discrimination in a Q-switched oscillator. The ASE of all these modes can be written as

$$I_{noise} = I_{ASE}\frac{\Delta v_{lase}}{\Delta v_{fl}} \quad , \tag{11}$$

where Δv_{fl} is the fluorescence bandwidth and Δv_{lase} is the actual Q-switched lasing bandwidth.

The contrast between the noise signal and the seeded mode can also be expressed in terms of the difference in build-up times between the seeded and noise mode as illustrated in Fig. 6.

$$Contrast = \frac{I_{seed}}{I_{noise}}\bigg|_{t=t_{constant\ rate}} = G_c^{\frac{\Delta t}{T}} \quad , \tag{12}$$

where the contrast is measured at a time when all curves have reached a constant slope as shown in Fig. 6. Also, G_c is the overall cavity gain including all losses, T is the cavity round trip time, and I_{seed} is the injected signal on resonance. If the seed signal is injected off resonance, I_{seed} and I_{noise} should be taken at an appropriate time when I_{seed} has shifted onto resonance.

III.3.   Spatial Hole Burning

The phenomenon of spatial hole burning occurs in a monomode laser when linearly polarized light resonates inside a standing wave cavity. Gain saturation occurs predominantly around the maxima of the standing wave inside the gain medium. This leaves a portion of the gain medium unsaturated allowing other modes to grow if their maxima fall near the nodes of the monomode wave. This effect is of particular importance in Nd:YLF oscillators as the medium is birefringent and forces linear polarization onto the modes.

Spatial hole burning in an injection-seeded slave oscillator then allows some "other" modes, growing from noise, to continue to grow beyond the time when the monomode pulse has reached its peak (Fig. 6). This can lead to a secondary multimode peak which follows the monomode pulse and which is wider due to the decreased available gain. As the monomode pulse only draws energy from only 1/2 of the geometrical mode volume its amplitude will be 1/2 that of the free running oscillators pulse. The secondary pulse due to spatial hole burning then contains the rest of the stored energy. A unidirectional ring cavity which only allows for a traveling wave in one direction circumvents this problem and gives the monomode pulse all of the stored energy in the mode volume.

III.4.   Mode Beating

Monomode laser output is desirable for its spectral purity and temporal smoothness which cannot be achieved by the randomly phased modes of a multimode laser. Mode beating is caused by two or more modes oscillating at different frequencies and interfering with each other. This creates a temporal structure of a sinusoidal to spiky nature depending on the number of modes involved and their relative phases.

The unseeded multimode pulse of the slave oscillator or the secondary multimode pulse due to the residual gain left over from spatial hole burning are made up of several modes which generally have statistically distributed amplitudes and phases. These modes add up to a more or less smooth output pulse with a low amplitude periodic (spiky) fluctuation superimposed on the pulse. If this pulse and the monomode pulse overlap in any way the result will appear to be the simple sum of the intensities. This is because the contrast between the monomode pulse and each of the individual modes in the secondary pulse is so high that mode beating effects are negligible.

In several cases, however, the observed sinusoidal structure is clearly identifiable as due to beating between the seeded mode and one of its two neighboring modes, suggesting that two modes have been seeded. This results in large sinusoidal amplitude fluctuations in the output pulse. In this case the injected signal, due to its finite bandwidth as well as the finite bandwidth of the exponentially growing Q-switch, seeds two modes simultaneously, resulting in the two modes of comparable magnitude (within a factor of 10 to 100) building up. This leads to much lower contrast than that relative to the modes growing from noise. The contrast between the two seeded modes then depends on the position of the seed signal between the two axial eigenmodes of the slave, and the relative time it takes for the seed signal to switch to each of the resonances. This is schematically illustrated in Fig. 8.
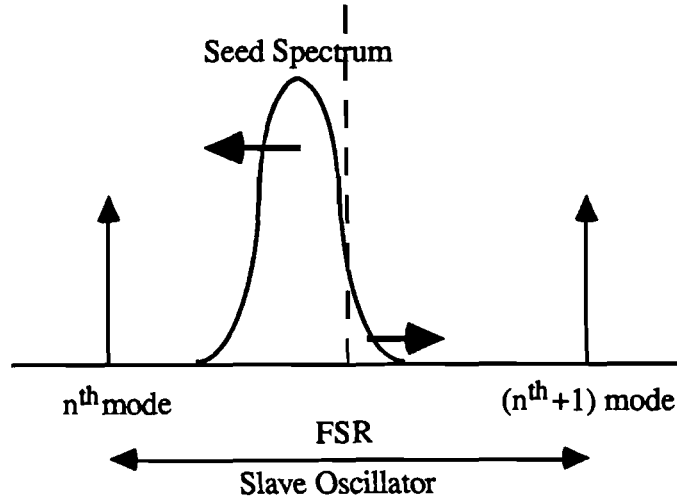
Fig. 8: Injection of a gaussian monomode pulse detuned off resonance so that it seeds two modes simultaneously. The injected signal is split proportionately between the two modes.

An interference analysis may be used to determine the beating between the two modes. An electric field traveling on axis in an optical resonator may be written as

$$\overline{E}_1(z,t) = \overline{A}_1(z,t)e^{-i(k_1 z - \omega_1 t)} . \tag{13}$$

A second electric field traveling inside the cavity may also be written as,

$$\overline{E}_2(z,t) = \overline{A}_2(z,t)e^{-i(k_2 z - \omega_2 t)} . \tag{14}$$

Summing the two electric fields and multiplying by their complex conjugate results in a total intensity circulating inside the cavity,

$$I_{tot} = A_1^2 + A_2^2 + 2A_1 A_2 \cos[(k_2 - k_1)z - (\omega_2 - \omega_1)t] . \tag{15}$$

The spatial variation in the cavity intensity is given by Δkz, and the temporal variation is given by $\Delta \omega t$. Such temporal variation on the output pulse is easily observed on an oscilloscope.

Figures 8 and 9 illustrate mode beating; Fig. 8 shows the mode beating between two gaussian pulses which are neighboring modes and peak simultaneously. The amplitude of the electric field of one gaussian is ten times that of the other. In Fig. 9 the same two gaussians are temporally separated by 50 ns and closely resembles typical experimental data for injection at frequencies well off-resonance (This is further discussed in Sec. V.2.).
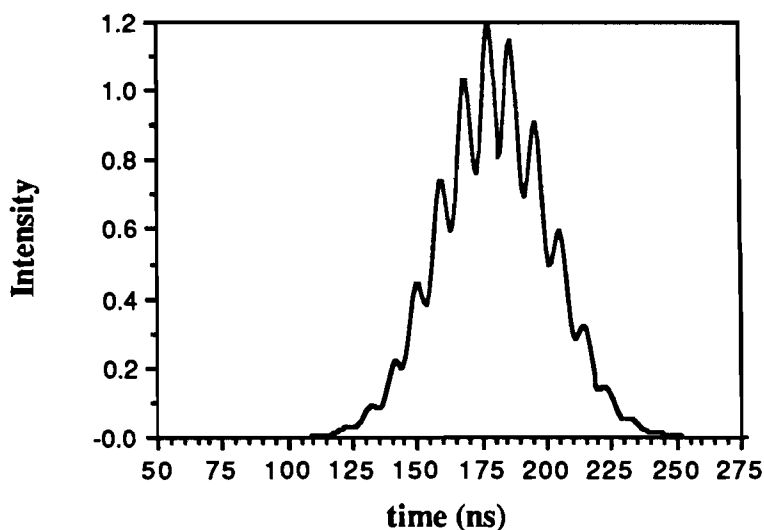
Figure 9: Two 30ns gaussian pulses of neighboring modes peaking at the same time with a 10:1 amplitude ratio.
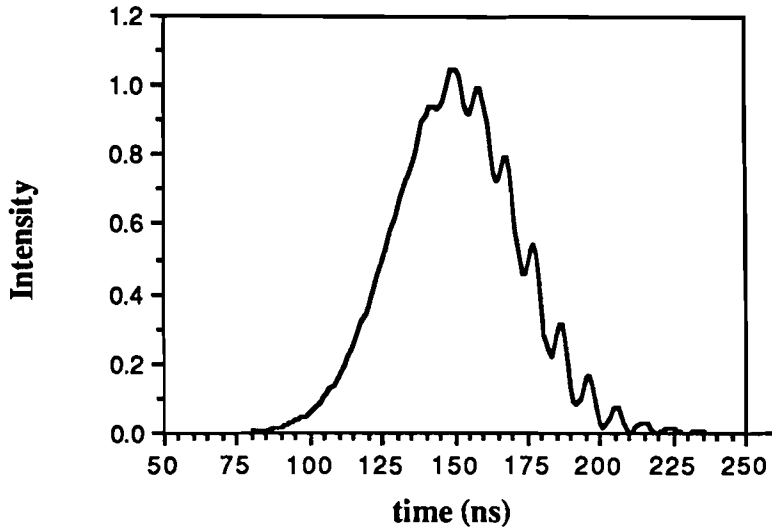
Figure 10: Two 30ns gaussian pulses or neighboring modes peaking 50ns apart with a 10:1 amplitude ratio.

IV.   Simulations

On the basis of the previous four sections we can simulate the evolution of injected signals numerically. By choosing an injection signal and either an immediate or finite Q-switch turn on time, Eq. (3) may be solved to obtain a buildup time, or contrast ratio, for an injected field whose frequency is detuned from the slave oscillators eigenfrequency. Results of this solution for different detuning angles are shown schematically in Fig. 7. If a linear line of constant intensity or time is drawn through all curves at a time when all growth rates have stabilized an estimate of relative buildup time or contrast may be made.

IV.1.   Simulation Results

This analysis will consider an electro-optic Q-switch having various turn on times and shapes. Depending on the seeding method, the Q-switch may not only modulate the cavity losses, but also the injected signal. This leads to a complex relationship between the

-18-

Q-switch and the seed pulse in determining the success of injection seeding. Three cases are studied in developing a working model of injection seeding. Case (1) illustrates an instantaneous Q-switch, while case (2) and (3) are more realistic (Fig. 11). Case (2) assumes a Q-switch which exhibits a contrast of 1000:1 within the cavity when turned off and whose transmission follows $T \propto \cos^2 \gamma t$, where γ is adjusted such that its 10%-90% rise time occurs over ten cavity round trips. The injected signal entering the cavity is modulated inversely and has values of unity before the Q-switch is turned on and zero when the Q-switch has completely turned on. Case (3) differs from case (2) only through a bias placed on the Q-switch voltage. This starts the cavity off with losses which are only 5% greater than the gain.
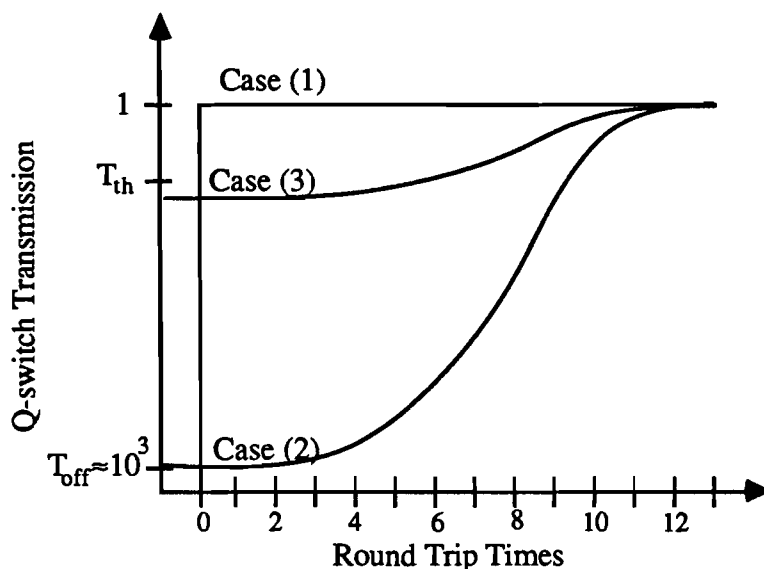
Figure 11: A schematic of the gain due to the Q-switch transmission vs. time as seen by the circulating signal inside the slave resonator. Case (2) assumes a Q-switch which exhibits a contrast of 1000:1. Case (3) assumes a Q-switch which results in the cavity being slightly below threshold when turned off and whose transmission varies as, $T \propto \cos^2 \gamma t$, so that its 10%-90% rise time equals 10 cavity round trips.

The results of the simulation are shown in Figs. 12 and 13 in terms of pulse buildup times. For each of the three cases three different gains are simulated. The time axis of all curves is offset such that the case having the fastest buildup time starts at zero. Converting the pulse buildup times to contrast can be done using Eq. (12).

IV.2. Comparison and Analysis

An immediate observation is that the pulse buildup time varies the least over the detuning range in the case of the immediate Q-switch and becomes greater for the biased Q-switch and greater yet for the high contrast Q-switch. Two factors account for this behavior: (1) how soon does the cavity see a net overall gain which results in the circulating signal switching onto the cavity resonance, and (2) how much constructive and destructive interference takes place between the injected signal and the circulating signal prior to the cavity going above threshold.

Once the cavity exhibits net gain (goes above threshold), detuned injected signals may begin their convergence to cavity resonance. The higher the gain, the faster the circulating intensity grows causing the injected signal to have a negligible influence on the cavity. At this point the circulating intensity is on resonance as discussed in Sec. II.3 and the buildup times are insensitive to the detuning of the injected signal.

If the Q-switch takes a long time to fully open, the signals having greater detuning angles will witness various amounts of destructive and constructive interference during the initial phases of the opening of the Q-switch. This interference is compounded on each round trip for which the circulating field is constrained in a cavity below threshold. This leads to a high amplitude contrast between a signal injected on resonance and the same signal injected far off resonance before the net cavity gain goes above unity. This contrast

(a)

Instantaneous Q-switch

(b)

Biased Q-switch

(c)

High Contrast Q-switch
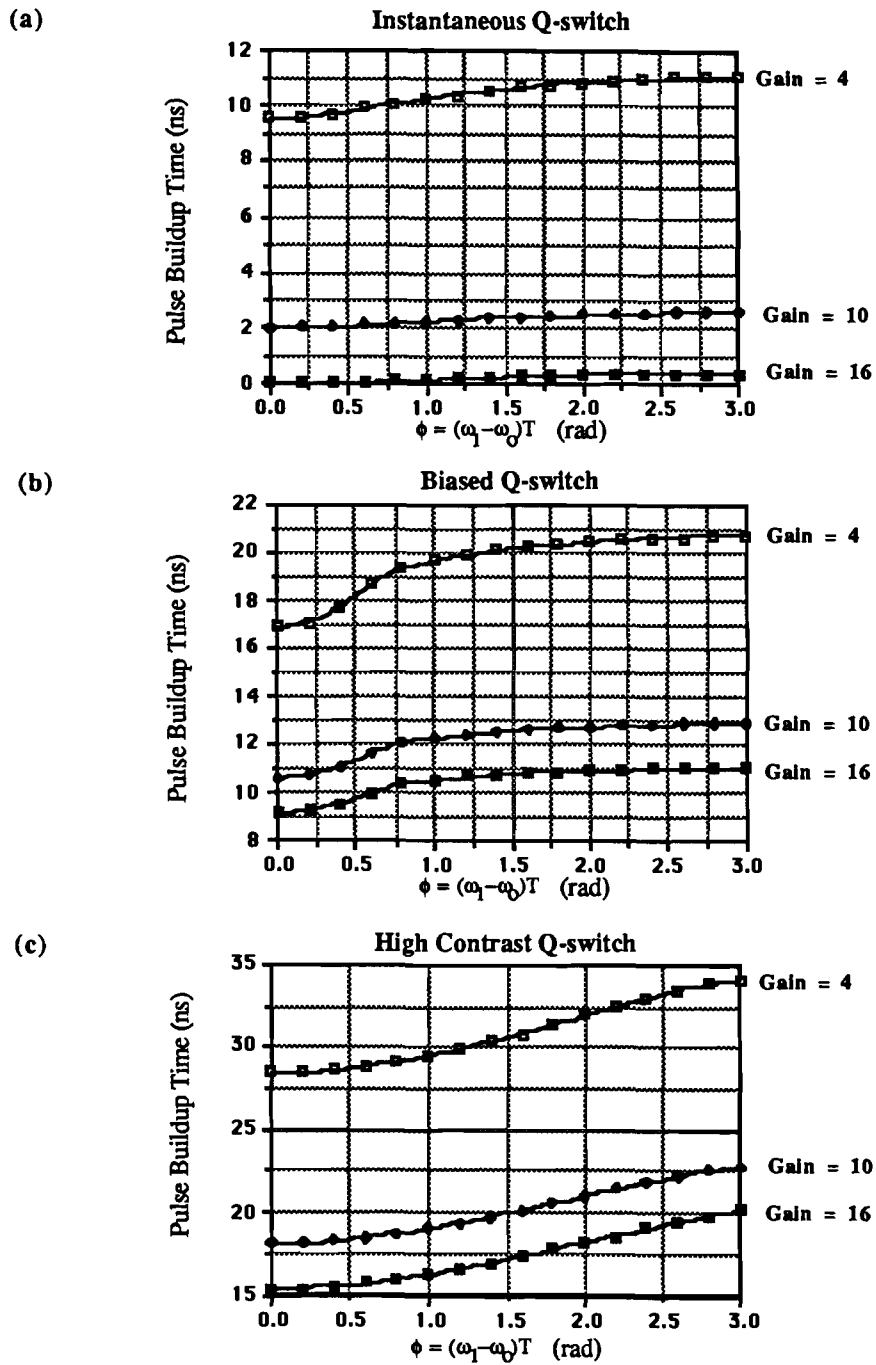
Figure 12: Pulse buildup time vs. detuning angle ϕ, where $\phi=(\omega_1-\omega_0)T$, for (a) instantaneous Q-switch and constant injection, (b) a Q-switch having high contrast and a slow turn on time, and (c) a Q-switch having lower contrast and a slow turn on time.

Comparison of Q-switch Methods
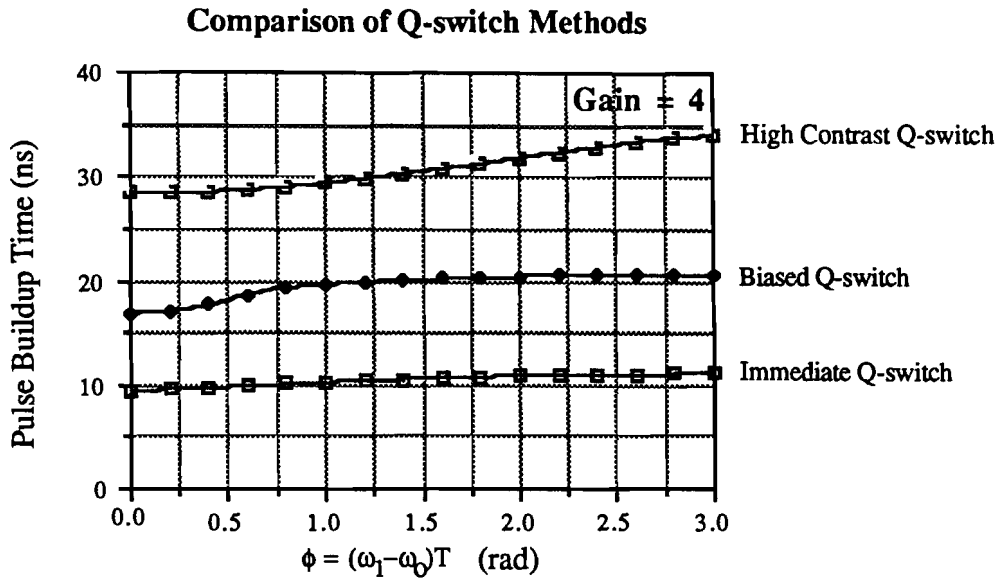
Figure 13: Comparison of Q-switch methods from Fig. 11 for a net gain of four.

is further increased by the time it takes for the signals to convert to resonance. These effects explain the large dynamic ranges of the curves for the more realistic cases in Figs. 12 and 13.

This analysis alone, however, is not sufficient in allowing us to define the optimal Q-switch turn on as it ignores spectral bandwidth. In the case of an injected signal with a finite bandwidth, the amplitude and phase modulation placed on the seed signal must be accounted for. This results in a spectral broadening of the seed pulse leading to the possibility of seeding of more than one mode if the seed is far enough off resonance. The faster the Q-switch rise time is, the greater the phase modulation placed on the frequency of the injected signal, and the greater the Q-switch contrast is, the greater the amplitude modulation leading again to spectral broadening. This broadening may account for the seeding of two modes simultaneously as discussed in Sec. III.3.

At first glance, the instantaneous Q-switch, case (1), looks best as the range of the pulse buildup time is the least; however, when considering the spectral broadening of the

injected signal due to a large intensity modulation and a fast intracavity phase shift caused by the rapidly switching Pockels cell, it is no longer the optimal choice as high contrast between neighboring modes may be hard to obtain. This conclusion has been verified experimentally (see Sec. V.2).

The high contrast Q-switch, case (2), incorporates a long turn on time resulting in a lower modulation of the phase, however, it imposes a large amplitude modulation on the injected signal resulting in increased spectral broadening. The long Q-switch turn on time results in repeated destructive interference leading to larger differences in build-up time between signals injected on and off resonance. This increases the contrast between neighboring modes when two modes are simultaneously seeded.

The biased Q-switch, case (3), utilizes a long rise time and minimal amplitude modulation of the injected signal. This leads to the least amount of spectral shift and spectral broadening to the seed pulse. The slow increase in cavity gain allows destructive interference to contribute to the dynamic range of the pulse buildup time vs. detuning range curve (Figs. 12 and 13). The results are a compromise between cases (1) and (2) with respect to the range of buildup times and a reduced spectral broadening of the injected pulse limiting the possibility of seeding neighboring modes. For these reasons the biased Q-switch is the best choice.

V. Experiment

The theoretical model developed in the previous section was experimentally investigated and verified using a monolithic Nd:YLF oscillator as the well controlled resonator, and a conventional, linear Nd:YLF Q-switched laser as the high power multimode oscillator to be driven monomode.

V.1. Experimental Apparatus

The injection seeding system is illustrated in Fig. 14. The system consists of a laser diode pumped Nd:YLF master oscillator, a permanent magnet faraday rotator, and a Q-switched Nd:YLF slave oscillator. The faraday rotator isolates the master oscillator from the slave to prevent optical damage and destabilization due to high power optical feedback from the slave.
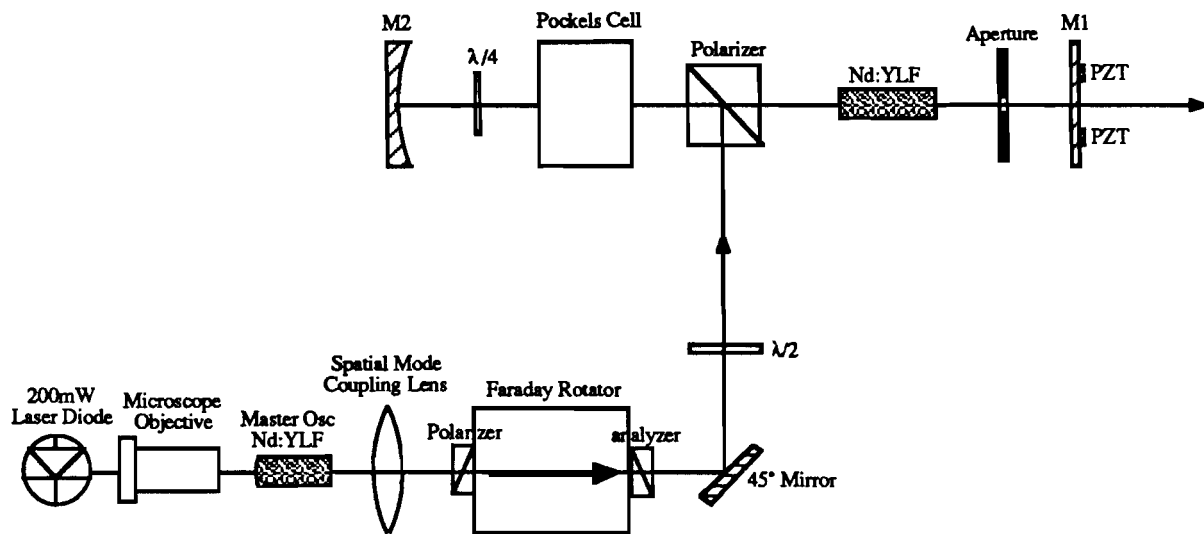

Figure 14: Schematic of injection seeding system

Nd:YLF was chosen because of its compatibility with glass amplifiers. Nd:YLF lases naturally polarized at λ=1047nm along the extraordinary axis (π polarization), and λ=1053nm along the ordinary axis (σ polarization). For the purpose of this study, the system was designed to run at at 1047nm as the gain is considerably larger than at 1053nm. Nd:YLF is a homogeneously broadened material and has a gain bandwidth (FWHM) of $\approx$12Å. The longitudinal modes which lase in the free running Q-switched oscillator typically fall in the top 10% of the bandwidth. The fact that Nd:YLF is birefringent with anisotropic gain creates a problem when using Nd:YLF in a standing wave oscillator as spatial hole burning cannot be avoided. This problem is circumvented in isotropic gain media by propagating circularly polarized light inside the active medium.

The master oscillator is a laser diode pumped monolithic Nd:YLF crystal which exhibits single mode operation both spectrally and spatially. The crystal is fabricated as a stable oscillator having a length of 2.5mm, a flat output coupler, and a back mirror with a 1cm radius of curvature (the rod diameter is 6mm). The output coupler has a reflection coefficient of 97% at 1047nm and a maximum reflectance at 792nm (the pump wavelength). The back mirror has a radius of curvature of 1cm, a maximum reflectance at 1047nm and a maximum transmission at 792nm. With an index of refraction of 1.4704 along the extraordinary axis a free spectral range of 41GHz or 1.49Å is calculated. This wide free spectral range combined with a slow pulse buildup time, limits the operation of the master oscillator to a single longitudinal mode as was verified experimentally using a 1m grating spectrograph. An end-pumping technique is used to limit the pump volume to the TEM_{00} mode. For temperature stabilization the master oscillator was placed in a brass heat sink (2" diameter x 1") The temperature of the master oscillator could be controlled to adjust the resonance frequency; however, this feature was not used in these experiments. The output of the master oscillator (Fig. 14) is a 500ns, 1nJ pulse. Spatially it is gaussian with a beamwaist of 31μ (FWHM).

The laser diode is a Spectra Diode Labs 10 stripe 200 mW diode. At room temperature it lases at 802nm and must be cooled to -4°C to reach the 792nm absorption band in YLF. The output power of the laser diode in our experiment ranges between 20mW and 40mW. The duration of the current is just long enough for the master oscillator to generate its first spike. The master oscillator is operated at a 1KHz repetition rate.
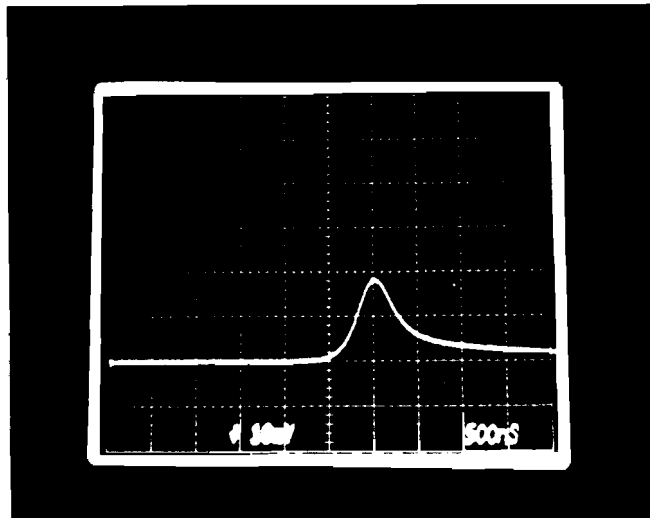
Figure 15: Photograph of Master Oscillator Pulse.

A 5x, 0.1NA microscope objective is used to couple the laser diode to the master oscillator. The pump beam is injected through the back mirror, carefully aligned with respect to the TEM_{00} mode volume, and imaged on the output coupler for optimal volume overlap.

The slave resonator is a conventional linear Q-switched oscillator. It has a length of 1.1m resulting in a longitudinal mode spacing (free spectral range) of 136MHz. Its end mirror has a 2m radius of curvature and R=98%. The output coupler is flat with R=40%. The active medium is a flashlamp pumped, water cooled, Nd:YLF rod with a length of 8cm and a 4mm diameter. No intracavity etalons are used to preselect the longitudinal modes,

and an aperture is used to limit the cavity to the TEM_{00} mode. The slave oscillator output is a few millijoules.

The master oscillator is spatially mode matched to the slave oscillator by a mode coupling lens. This lens images the beam waist of the master onto the beamwaist of the slave to obtain optimal overlap of the gaussian modes. The longitudinal modes are matched with a piezo-electric translation stage mounted to the output coupler of the slave oscillator.

The Q-switch (consisting of a KDP Pockels cell, a quarter wave plate, and a polarizer) is triggered by the master oscillator pulse. It has a 100ns turn on time and contrast of approximately 1000:1 when in the high loss mode. The voltage applied to the Q-switch, Fig. 16, determines its transmission, $T = cos^2(\pi/2 * V(t)/V_{max})$.

Two fast oscilloscopes along with a fast photodiode, and a Fabry Perot interferometer were used to evaluate the monomode operation of the slave oscillator. A Tektronix 7104 and 7832 storage scope were used to monitor the buildup time and the mode beating, if any, between oscillator modes. The slave oscillator output was frequency doubled and a $1cm^{-1}$ Fabry Perot with a finess of 60 at 523.5nm was used as a visual monitor.
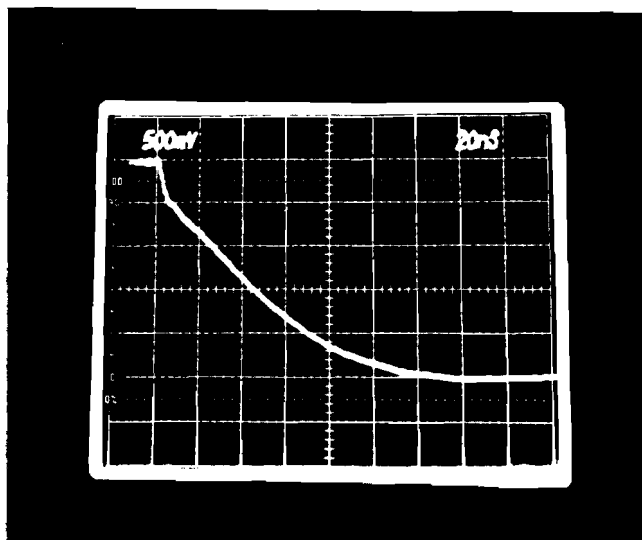

Figure 16: Voltage measured across the KDP crystal in the Pockels Cell. Full $\lambda/4$ voltage=4KV

V.2.   Experimental Results

The free running slave oscillator output is shown in Fig. 17: the pulse is made up of many longitudinal modes causing the spiky appearance evident in the figure. Figures 18 - 20 show the slave oscillator output with injection seeding at various detuning frequencies. In monomode operation we see a shortening in the buildup time followed by a second multimode pulse due to spatial hole burning. Notice that the second pulse is wider than the first as a result of the expected reduction in the overall gain for the secondary pulse. In the discussion of mode beating (Sec. III.3) a difference was noted between the mode beating due to the sum of all the modes making up the secondary pulse and the mode beating between two neighboring modes of comparable size (intensity contrast 100:1). Figure 19 and 20 illustrate this difference. In the former we see mode beating between the monomode pulse and the secondary pulse. This essentially results in the sum of the intensity of the two pulses. Figure 20, however, illustrates the case where two neighboring modes have been seeded simultaneously. Note that the shorter the buildup times for the monomode pulse are always paired with longer buildup times for the secondary pulse. Figures 21 and 22 show the monomode and multimode pulses at a higher resolution while keeping the temporal relationship between them.
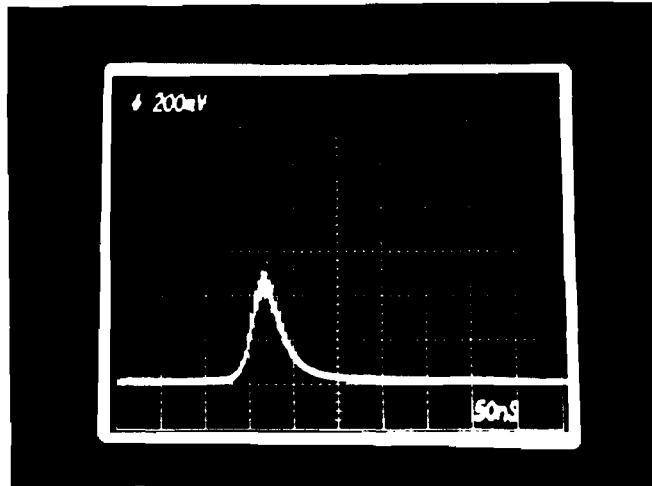
Figure 17: Multimode slave output pulse on a 50ns/div scale.
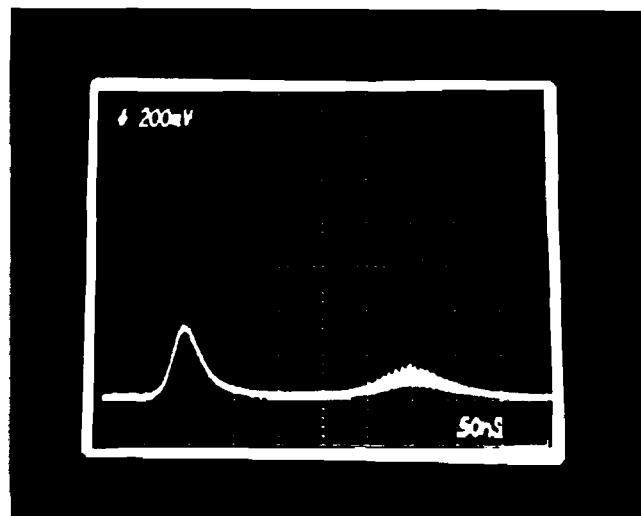
Figure 18: Monomode slave output from optimal injection seed, 50ns/div scale.
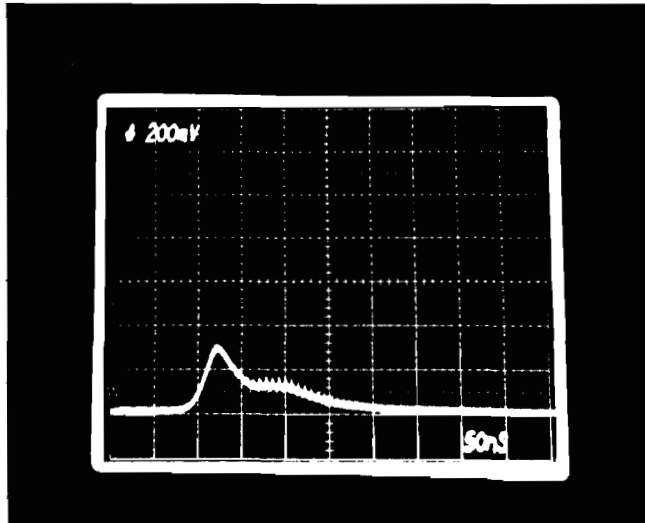
Figure 19: Monomode slave output from detuned injection seed. Notice how trailing pulse creeps up on monomode pulse. (time scale= 50ns/div)
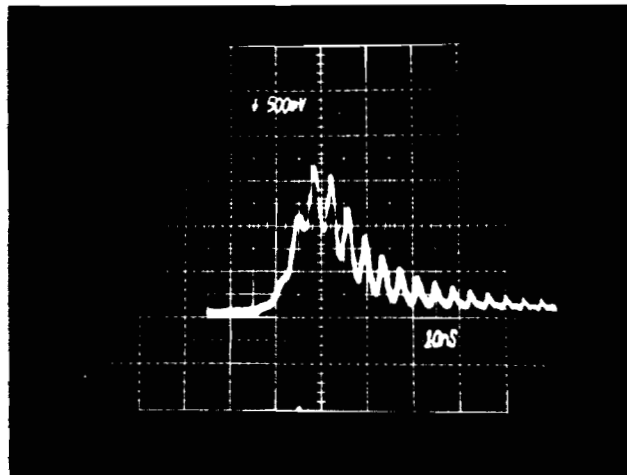
Figure 20: Two neighboring modes beating due to the seeding of both modes. (time scale=10ns/div)
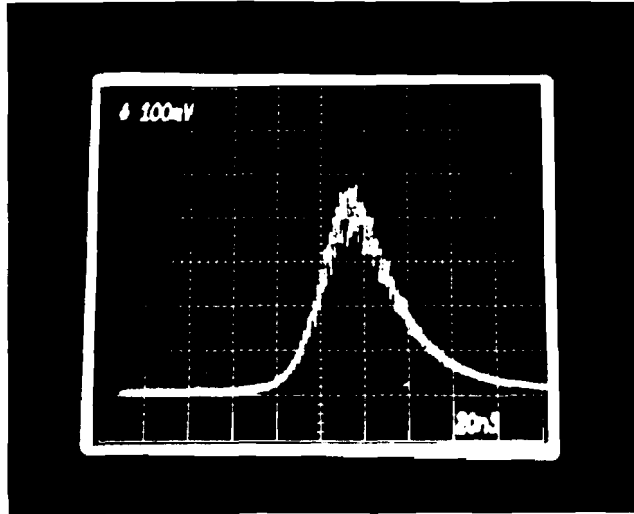
Figure 21: Multimode slave pulse on an expanded scale, 20ns/div.
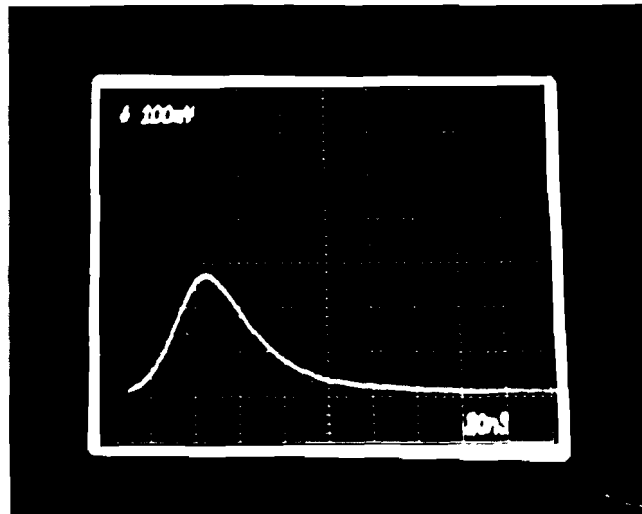
Figure 22: Monomode slave pulse on an expanded scale, 20ns/div.

The experimentally obtained differences in pulse buildup times over a range of injection frequencies is shown in Fig. 23. The first plot shows the results for an overall gain of 4 and the second for an overall gain of 16. Each experimental point represents the average of three shots. The experimental results are biased so that t=0 represents the monomode pulse for which the injection seed was on resonance. Good agreement between the data and the simulation is evident from this figure. The injection seeding range over which the output was purely monomode was $\approx$30% of the free spectral range for the case when the gain was four and $\approx$25% of the free spectral range for the case when the gain was sixteen and is shown as a horizontal line in Fig. 23.

Up to this point we have neglected the energy of the seed signal. The dynamic range of the curves in Fig. 23 may be verified through the contrast analysis in the ASE section. The seed pulse has an energy of 1nJ or a power of $\approx$0.2W/cm^2. The competing noise signal due to ASE (Eq. 11) is I_{noise}=1.6 x 10^{-5} W/cm^2 for a cavity with an overall round trip cavity gain of 4 (G_0=3.37) and I_{noise}=4.5 x 10^{-5} for an overall round trip gain of 16 (G_0=6.73). This results in contrast ratios of 5,800 and 1,850 respectively. The variation in pulse buildup time between the free running oscillator with no seed and the injected seeded pulse is 46ns for the cavity with an overall gain of 4 and 22ns for the cavity with an overall gain of 16. This is in good agreement with the Fig. 23.

(a)

Gain = 4

(b)

Gain = 16
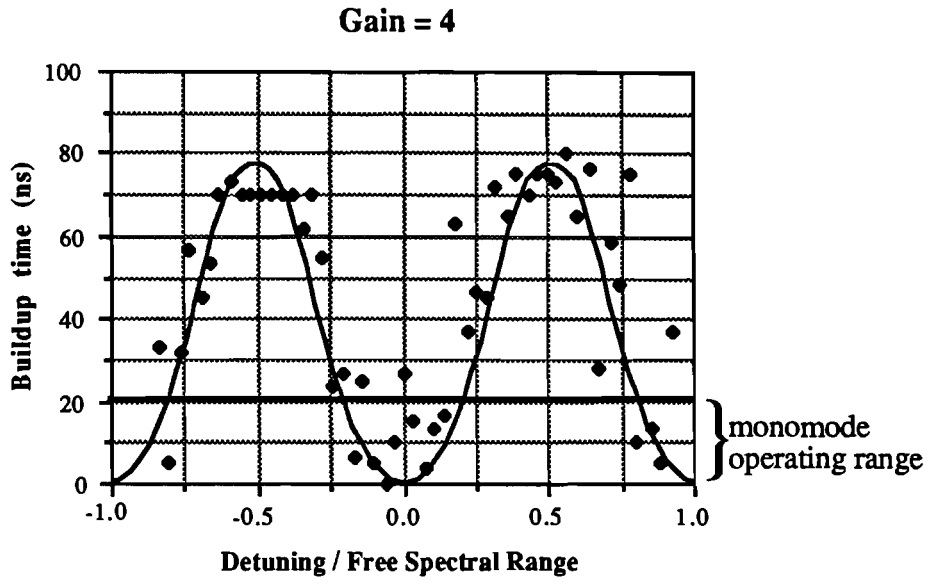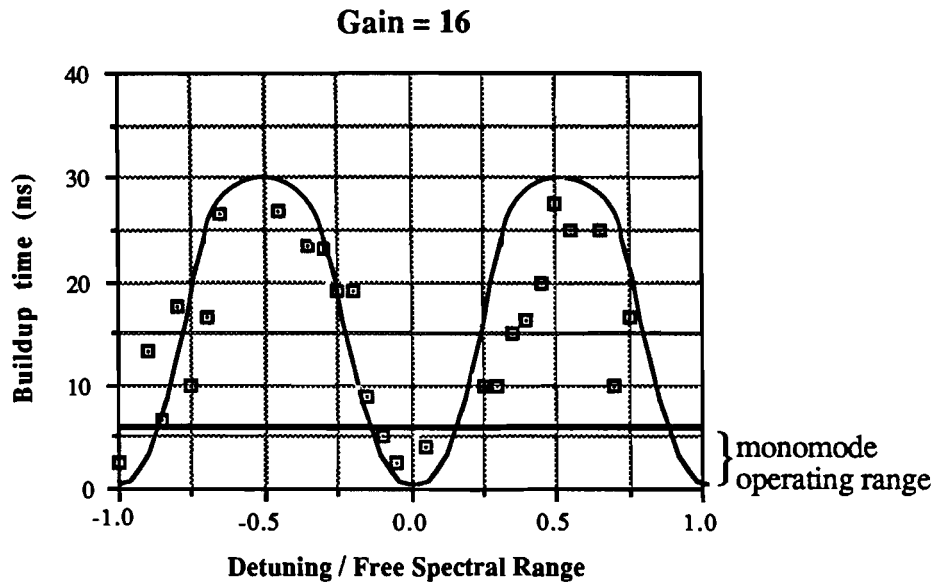
Figure 23: Experimental data over two free spectral ranges for two different gains. Curve (a) was taken at

an overall gain of 4 while curve (b) represents an overall gain of 16.

VI. Recommendations for Future Improvements

This study confirms the success of injection seeding in achieving monomode operation in high power Q-switched oscillators. The present study, however, has also brought out a number of problem areas which impede optimum monomode operation of the present system. In this section the shortcomings are addressed and alternatives suggested.

VI.1. Ring Oscillator

The trailing multimode pulse, resulting from spatial hole burning may be eliminated by converting the linear oscillator into a unidirectional ring oscillator. The Faraday Rotator may be mounted inside the ring oscillator to eliminate the formation of a standing wave. Additional advantages to this design are low power feedback to the master oscillator and, as illustrated in appendix A and discussed in Sec. II, a ring oscillator allows for the most effective seeding method. A suggested configuration is illustrated in Fig. 24.
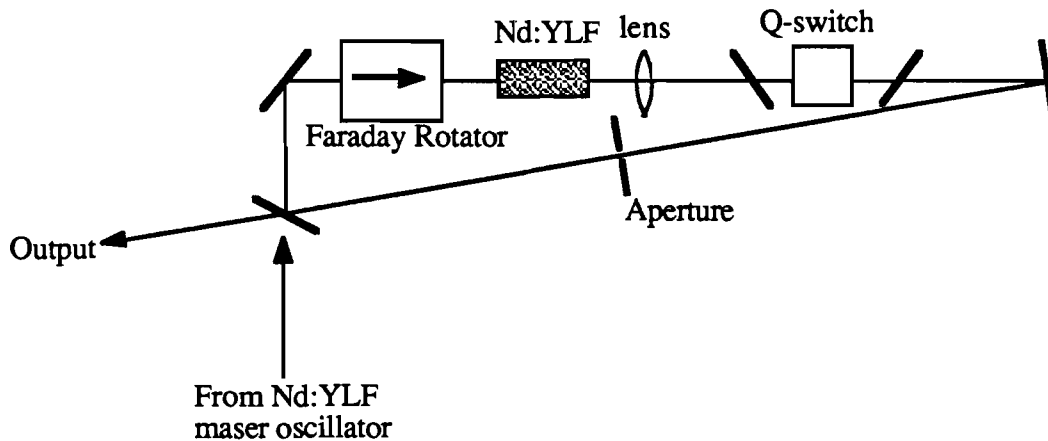
Figure 24: A ring oscillator for optimum injection seeding.

VI.2. Master Oscillator Stabilization

In our experiments a 15%-25% amplitude jitter and a .5µs to 1µs temporal jitter of the output of the master oscillator were observed. This may be linked to the thermal control of the laser diode. The 200mw laser diode used in these experiments has a 1.5nm spectral bandwidth when run at 80mW and its frequency varies by 0.3nm/°C. The Nd:YLF absorption band, shown in Fig. 25 (the sample was a 5mm YLF chip cut from the same crystal as the master oscillator), shows a narrow absorption peak at 792nm which is on the same order as the pump spectrum of the laser diode. A spectral shift in the laser diode output resulting from thermal instability of ≈1°C can account for the observed jitter in our experiments. This is further analyzed in Appendix B.
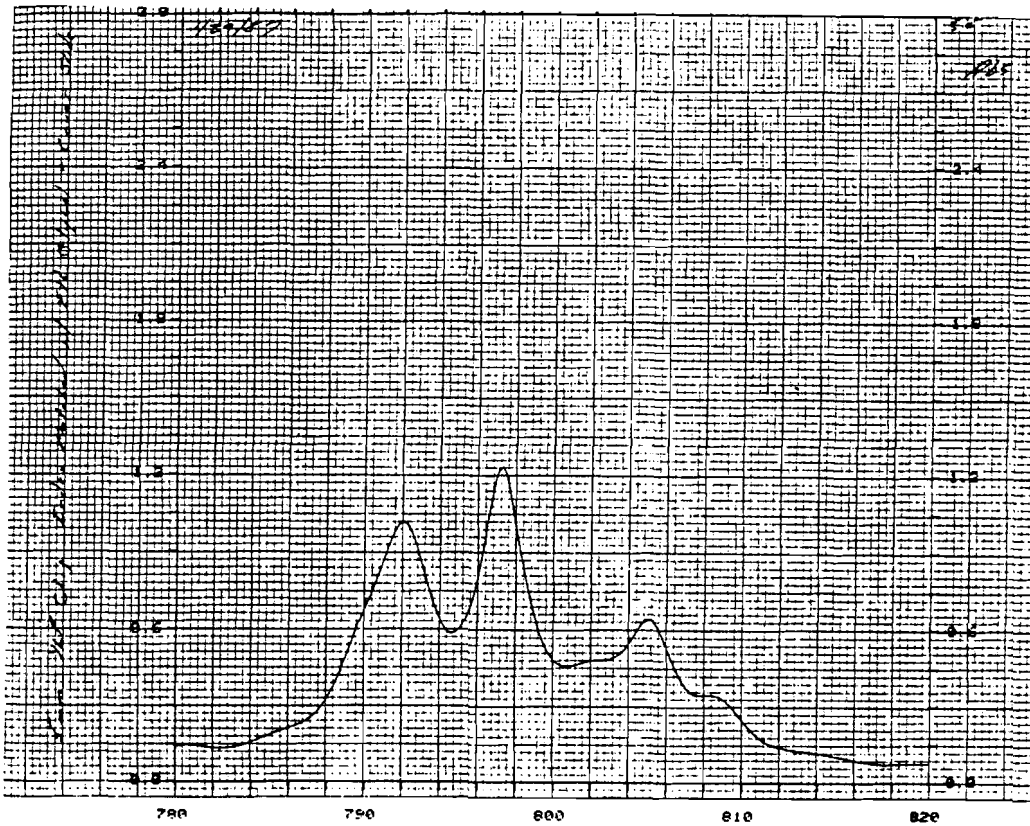
Figure 25: Absorption curve for 5mm Nd:YLF crystal. The units for the vertical axis is optical density .

VI.3.   Active Stabilization

Successful long term injection seeding requires the output frequency of the master oscillator and the slave oscillator be held as close as possible. Detuning these values past those specified in Sec. V and shown in Fig. 23, results in unsuccessful injection seeding. An error signal which determines the detuning between the two frequencies can be used to automatically adjust the cavity length of the master or slave oscillator so that the seed lies on a resonance of the slave oscillator. Previously, two fundamentally different feedback techniques have been used. The first measures the pulse buildup time [13] which is directly related to the cavity detuning as shown earlier. In searching for shorter buildup times one can employ a dithering technique of the slave cavity length which varies the resonance and thus the buildup times around its optimum value. Alternatively, the slave oscillator may be locked slightly off resonance resulting in a signed error signal. In another feedback technique a Fabry Perot etalon is used to determine the detuning between the master and slave[14-16]. Park et al.[8] have locked both the master and the slave oscillator to an external etalon, requiring careful temperature stabilization of a third etalon. Teets[14] observed an increased intensity through the rear reflector of the master oscillator when the incident signal was on resonance. This results in a symmetric signal about the optimum and consequently requires dithering or locking slightly off resonance. Teet's scheme is also difficult to implement in an end-pumped system as it requires access to the back mirror of the master oscillator. Esherick and Owyoung[15], on the other hand, utilized the slightly birefringent master oscillator as a reflecting reference cavity to derive an asymmetric error signal eliminating the need for dithering or locking off resonance. This method was first discussed by Hansch and Couillaud[16]. This error signal is obtained by allowing the on-resonance polarization signal to heterodyne with the phase shifted orthogonal polarization. In Ref. [15] a mechanical strain was applied to the Nd:YAG master oscillator causing

birefringence in the crystal and resulting in the two orthogonal polarizations having slightly different resonance frequencies. Since Nd:YLF is birefringent, it naturally lends itself to this technique.

The asymmetric error signal is obtained by allowing a small amount of the slave output to feed back through the Faraday Rotator. The Faraday Rotator separating the master from the slave oscillator is located to the right of the polarizer shown in Fig. 26. The direction of polarization (π) of the master oscillator relative to the fast axis $\hat{x}'$ of the quarter wave plate is given by the angle θ. The angle between the fast axis of the wave plate and the orientation of the polarizer $\hat{x}$ is given by ϕ. When $\phi=0$ the effects of the quarter wave plate can be ignored. Error signals obtained under these conditions where $\phi=\theta=10°$ and the resonance splitting is FSR/8 are shown in Figs. 28 and 29.
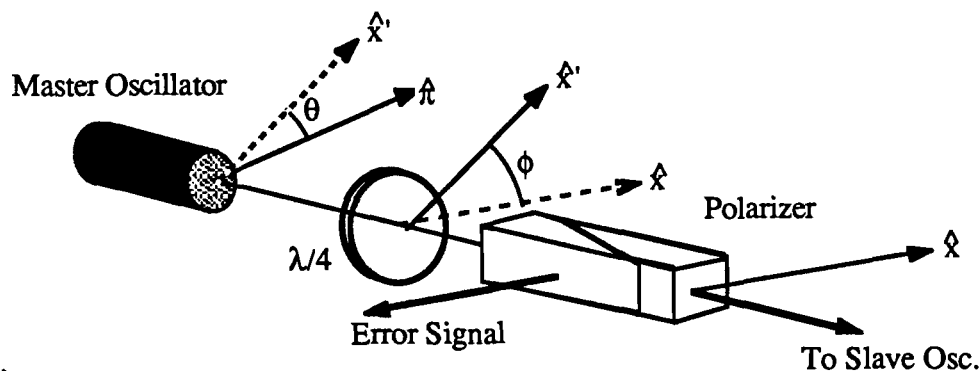
Figure 26: Schematic of optical components used in deriving the error signal.

(From Ref. 15, by permission of the authors)

A birefringent etalon may be treated as two separate Fabry Perot etalons with the incoming signal split into its two orthogonal components. The two etalons have different optical path lengths requiring careful accounting of the phases for the two polarizations. It is convenient to use the results
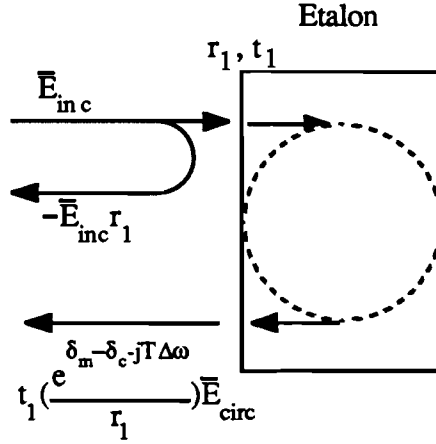
Figure 27: Model of a Fabry Perot etalon (by permission of author[17]).

of Sec. II.2 to analyze the behavior of such an etalon with or without a gain medium inside. Figure 27 illustrates a typical Fabry Perot etalon. The total electric field reflected by an etalon from a signal incident upon it is described by Eq. (17). This consists of the straight forward reflection (phase shifted by 180°) off the front surface and the transmitted portion of the circulating signal,

$$\bar{E}_{ref} = -\bar{E}_{inc}r_1 + t_1 \left(\frac{e^{\delta_m - \delta_c - jT\Delta\omega}}{r_1} \right) \bar{E}_{circ} \ . \tag{16}$$

The circulating field, derived in Eq. (4), may be rewritten as,

$$\bar{E}_{circ} = \frac{t_1 \bar{E}_{inc}}{1 - e^{\delta_m - \delta_c - jT\Delta\omega}} \ , \tag{17}$$

where $\bar{E}_{inj}$ has been replaced by $\bar{E}_{inc}$ which is measured outside the cavity . The phase term

reflects the detuning $\Delta\omega$ between the master and slave lasers. Combining Eqs. (16) and (17) gives the amplitude reflection coefficient of the cavity,

$$r = \frac{\bar{E}_{ref}}{\bar{E}_{inc}} = \frac{1}{r_1} \times \frac{-r_1^2 + e^{\delta_m - \delta_c - jT\Delta\omega}}{1 - e^{\delta_m - \delta_c - jT\Delta\omega}} \quad . \qquad (18)$$

In a cold Fabry Perot, containing no gain, the reflectivity is found to be a maximum when the incident signal is off resonance by $\pi/2$ radians. This situation is reversed to a maximum reflectance on resonance when the product of the cavity gain and the back mirror reflectivity result in a value greater than unity. Typically, after the master oscillator lases the gain is just below threshold satisfying this condition. In the case of the master Nd:YLF oscillator lasing at 1047nm we find $r_\pi(\omega)$ (lasing in the π polarization) is a maximum when the incident signal is on resonance. The orthogonal polarization, $r_\sigma(\omega)$, has no gain, resulting in a minimum reflectance on resonance.

Given a birefringent etalon with reflectivities $r_\pi(\omega)$ and $r_\sigma(\omega)$ for the two orthogonal polarizations the error signal at the photodetector (Fig. 26) is

$$\text{Signal} = (\frac{I_o}{4})|[r_\pi(\omega) + r_\sigma(\omega)]\sin2\phi + j[r_\pi(\omega) - r_\sigma(\omega)]\sin2\theta\cos2\phi|^2 \quad . \qquad (19)$$

The simulated error signals for our experimental setup are shown in Figs. 28 and 29. The signal is computed for $R_1 = r_1^2 = 0.98$, $R_2 e^{2\delta_m} = 1.01$, $\theta = \phi = 10°$, and we assumed a mode splitting is 1/8 the free spectral range. The simulated signal is normalized to $I_o/4$. The lasing axis (π polarization) resonance, defining the frequency of the injected signal, is centered about the zero value of the detuning angle/free spectral range. Fig. 29 shows the error signal plotted at a higher resolution.

In the Nd:YAG system from Ref. 15, the mode splitting between the two orthogonal axis was directly related to the amount of strain applied to the rod. Since Nd:YLF is birefringent no strain is required, however, the amount of splitting depends on the optical path length inside the crystal; we therefore do not necessarily know the frequency splitting. Heating the rod, however, changes the frequency splitting; a temperature change of $\approx21°C$ will change the splitting by 1/2 of a free spectral range. Computer simulation for a good error signal shows that the frequency splitting between the polarizations should be greater than 1/250 of the free spectral range or the error signal looses its useful asymmetry but this is the only constraint on the frequency splitting for a useful error signal.

The only difference between the error signal calculated for the Nd:YAG system and the Nd:YAG is the lack of symmetry about the center of the mode splitting. In the Nd:YLF system the gain in the two orthogonal directions is similar resulting in a symmetrical plot. In Nd:YLF, however, this is not the case. The lack of gain in the σ polarization results in a minimum reflectance for incident signals on resonance. This explains the small error signal about the σ polarization resonance.
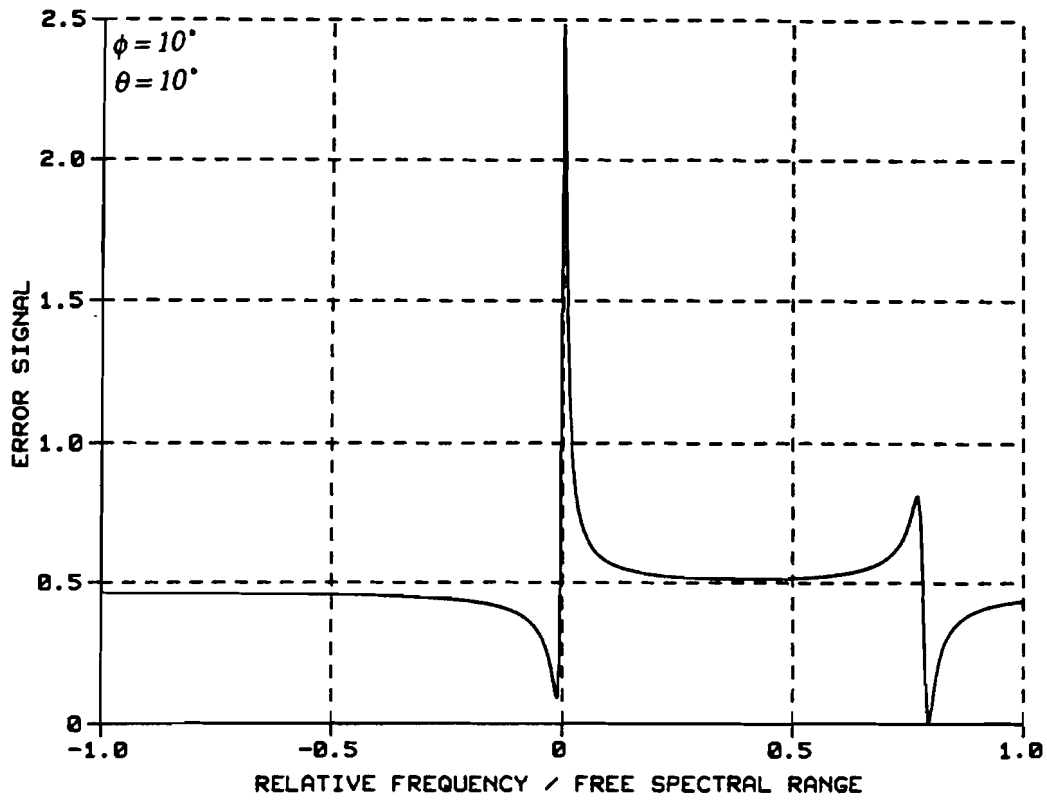
Figure 28: Simulation of the error signal
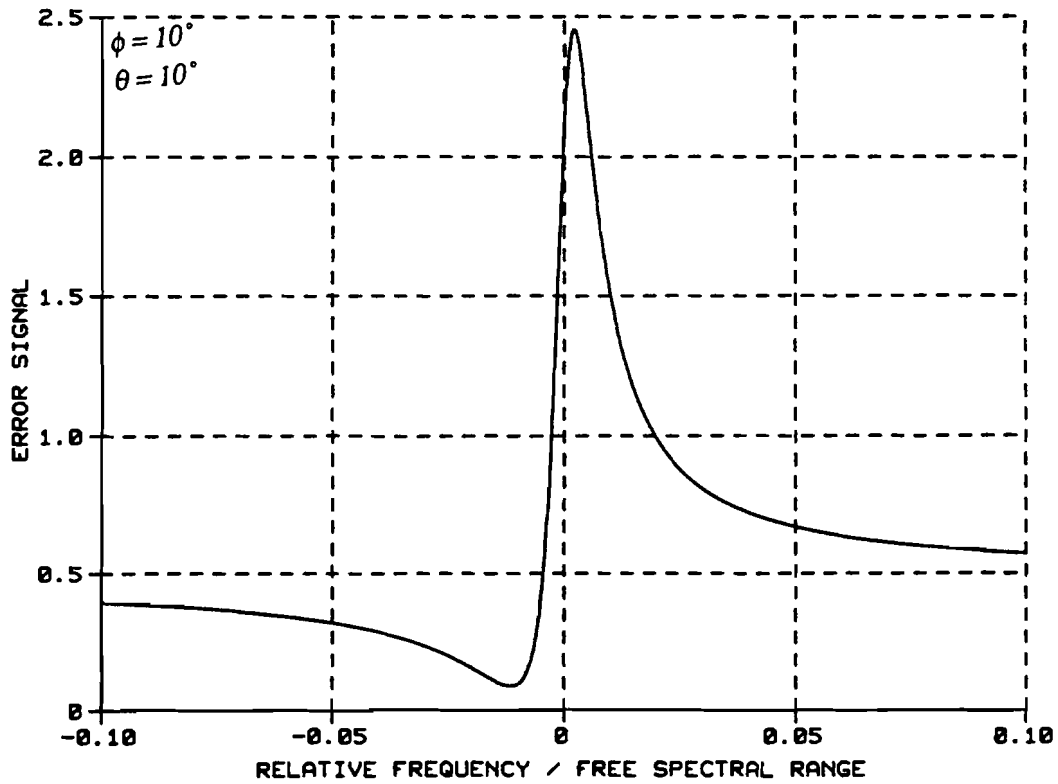
Figure 29: Higher resolution simulation of the error signal

-41-

VII. Conclusion

In this report we have analyzed and determined the operating parameters for successful injection seeding and mode selection in a Q-switched oscillator. A 1nJ, 500ns, monomode pulse from a laser diode pumped mini Nd:YLF oscillator was injected into a Q-switched oscillator producing reliable 30ns monomode output pulses having millijoule energies.

Spatial hole burning was found to be a limiting factor in our design. The use of a linear standing wave cavity with a Nd:YLF gain medium (birefringent with anisotripic gain) resulted in a secondary multimode pulse following the monomode pulse. A ring cavity permitting only a unidirectional traveling wave would solve this problem.

The seeding of two neighboring modes simultaneously is a result of spectral broadening of the injected pulse and a small dynamic range in the pulse buildup time vs. detuning angle curve. This situation is different from spatial hole burning and consequently cannot be eliminated by a unidirectional ring cavity. Implementation of a Q-switch with a long rise time minimizes spectral broadening of the seed pulse and enhances the development of large dynamic ranges (large differences in buildup times) between on and off resonance seed pulses. This enhances mode control of the slave oscillator and leads to the seeding of two modes simultaneously only when injecting well off resonance.

The data reported here are in good agreement with the simulations based on existing theory. On the basis of this analysis and simulation, the optimum injection method involves injecting through the output coupler of a unidirectional ring laser with a biased Q-switch of slow rise time.

Appendix A: Injection Methods

As discussed in the Sec. IV, the Q-switch transmission function determines the amplitude modulation placed on the injected seed signal. This modulation plays a key role in determining the successful monomode operation of the slave oscillator. Here we discuss four injection alternatives applied to a linear oscillator (Fig. 30) and show their respective results (Figs. 31 and 32).

In the transient injection seeding regime our simulation showed that the seed signal only influences the slave oscillator for a short period of time at the beginning of the pulse buildup (when the gain goes above threshold). Once the circulating signal inside the cavity becomes large compared to the injected signal, the injected signal no longer plays a role in the pulse buildup in the slave oscillator. It was also shown that larger injection seeds lead to higher contrasts between the seeded mode and the other (noise) modes oscillating in the slave resonator.
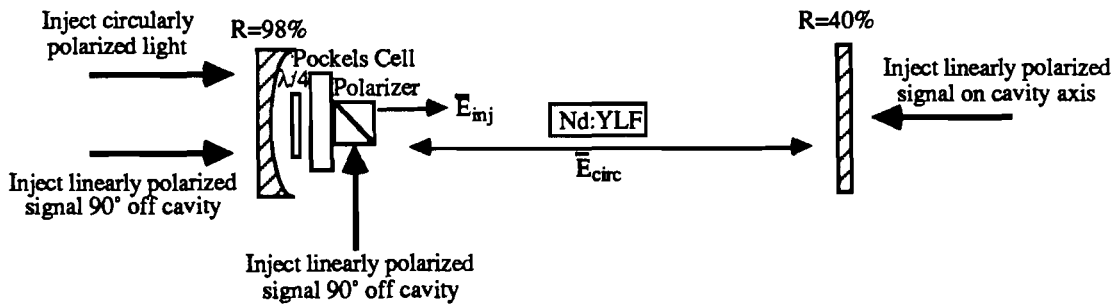

Figure 30: Four available injection options.

In this analysis we will group the Q-switch and end-mirror together (Fig. 30) to form the back surface of the cavity. The injected or circulating signal then sees the back surface of the cavity as made up of the back mirror reflectivity and the Q-switch

transmission at a given time. Injection into the cavity may take place through the output coupler, the back mirror (circularly or linearly polarized light), or the Q-switch polarizer.

Injection through the output coupler results in a maximum injection intensity when the Q-switch is turned on. Injection through the Q-switch polarizer leads to a modulation in the seed intensity resulting in $\approx 98\%$ of the injected signal entering the cavity when the Q-switch is turned off and no seed intensity when the Q-switch is on. Injection through the back mirror may be done in two ways. Injection of a linearly polarized signal (perpendicular to the lasing polarization of the slave cavity) results in $\approx 1\%$ of the signal entering the cavity before the Q-switch is turned on and 2% when the Q-switch is on. Finally, injection of circularly polarized signal results in $\approx 2\%$ of the light entering the cavity when the Q-switch is off and $\approx 1\%$ when the Q-switch is on.

For this simulation, the high contrast Q-switch discussed in Sec. IV and the experimentally measured Q-switch (Fig. 16) are used. The overall cavity gain is assumed to be four, and the curves (Figs. 31 and 32) are offset such that the curve with the shortest buildup time is set to zero. Each of the four different seeding methods show essentially the same difference in buildup time over the full detuning range. This spread is due to interference during the long turn on time while the cavity is below threshold (Sec. IV.2). The difference between the curves is a vertical displacement illustrating a constant change in buildup time. This difference gives preference to one option over the others as buildup time directly relates to the contrast of the monomode pulse.
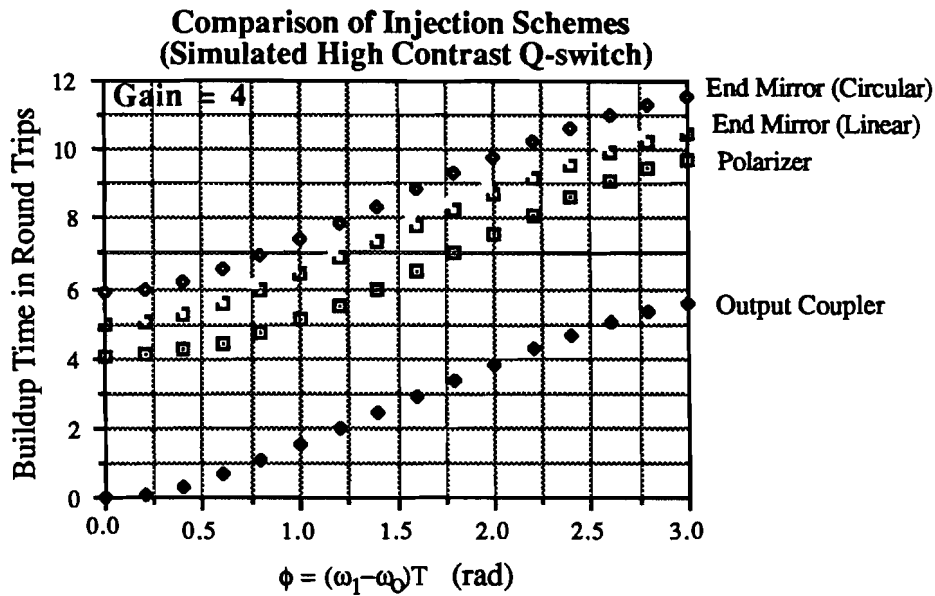
Figure 31: Comparison of four different injection methods. The Q-switch has a 1000:1 contrast ratio and transmission $T\alpha\cos^2\gamma t$, where γ is adjusted such that its 10%-90% rise time equals 10 cavity round trip times.
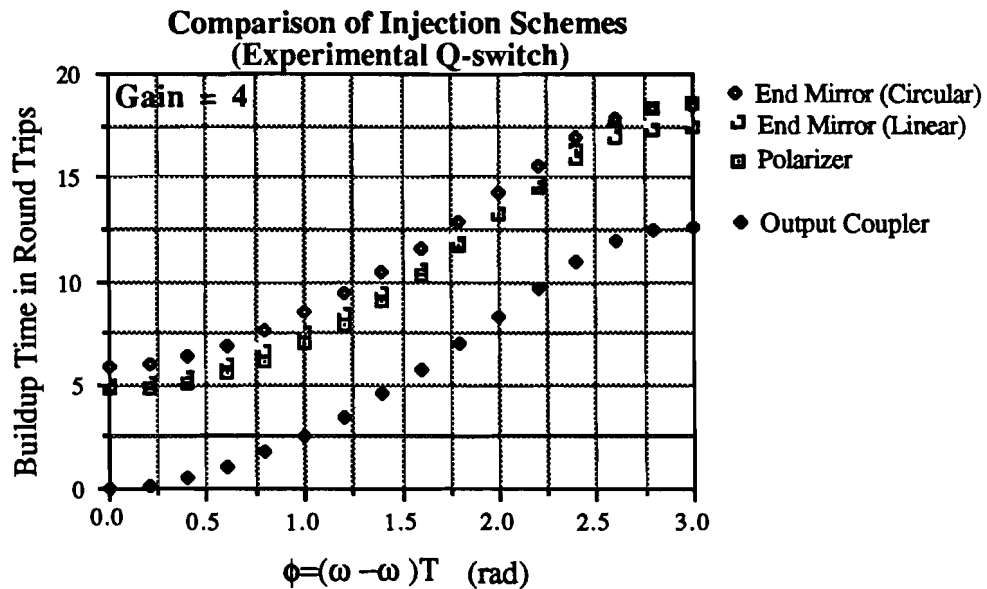
Figure 32: Comparison of the four different injection methods. The voltage to the Q-switch was measured experimentally and is shown in Fig. 15. The Q-switch transmission is $T=\cos^2(\pi/2*V(t)/V_{max})$.

The first injection method we implemented, an uninformed guess, was that of circularly polarized light through the end mirror. This resulted in small variations in pulse buildup time from that of the free running slave oscillator and no observed monomode pulses. Changing to injection through the polarizer we immediately obtained monomode operation and much shorter pulse buildup times which were in agreement with Figs. 31 and 32.

The difference in pulse buildup time between the seed pulse through the polarizer and the end mirror (circularly polarized case) is approximately two round trips. A look at the experimental data (Fig. 23) shows that a shift of the horizontal line (injection seeding range) down by two round trips all but eliminates the possibility of successful injection seeding. Only at low gains is monomode output possible and the detuning range is very small.

We concluded that injection schemes allowing faster buildup times are advantageous as they increase the allowable detuning range for successful injection seeding. They also allow lower injection energies. While increased overall gain also reduces buildup time, it is generally detrimental to monomode operation.

Appendix B: Laser Diode Control

The narrow band end-pumping scheme employed in pumping the master oscillator is elegant and efficient. Successful implementation, however, requires critical spectral overlap between the pump and absorption bands. In our experiment a 0.5µs to 1µs temporal jitter and a 15% to 25% amplitude jitter in the master oscillator output was observed. Improvements to these problems are outlined below.

A 200mW, 10 stripe, laser diode running at 802nm at room temperature was used in the experiment. The variation in wavelength with operating temperature was 0.3nm/°C. Experimentally the diode was found to pump the 792nm absorption band in Nd:YLF most efficiently at -4°C and was pulsed between 40mW and 80mW CW power. The bandwidth of the laser diode output was 1.5nm at 80mW. The Nd:YLF absorption band at 792nm (Fig. 25) is not much larger than the laser diode pump bandwidth, placing a tight tolerance on the spectral control of the pump source. If the laser diode fluctuates in temperature by $\approx 1°C$ the master oscillator's jitter is easily accounted for.

In optimizing thermal control over the 10 stripe laser diode the temperature controller must keep the laser diode within a 0.1°C of the set temperature. Two variables which aid in this task are proper heat sinking and optimization of current to the thermoelectric cooler. Proper heat sinking is important for heat dissipation of the laser diode. The temperature of this laser diode may fluctuate 10°C when turned on. It is therefore necessary to remove the heat efficiently so that it does not bottleneck forcing the diode to higher temperatures. Secondly the current to the thermoelectric cooler may be optimized experimentally to give the most efficient cooling. Thermoelectric coolers are specified with a maximum current that may be applied, however, the necessary current to most effectively cool is dictated by the particular application. It may not be best to draw the maximum amount of heat in the minimum time. Different forward currents and pulse

lengths to the laser diode my require different operation of the thermoelectric cooler in optimizing the laser diode cooling.

The best alternative, however, is to select a laser diode which operates close to the pump band at ambient temperature. This limits the necessary thermal control over the laser diode, decreasing the importance of the thermal controller.

It may be advantageous to replace the multistripe laser diode with a single stripe diode. Because Nd:YLF has a fairly low threshold, a lower power diode such as a single stripe 20mW laser diode is sufficient. Advantages to this are better spectral control and decreased bandwidth.

Appendix C: Pulse Buildup Time Simulation

The program used to simulate the buildup time vs. detuning angle is listed below.

This program assumes a high contrast Q-switch having the transmission function described

in Sec. IV.

```
******************************************************************************
      PROGRAM DETUNE
******************************************************************************

*****************************
*     EC=circulating field        *
*     ER=real part of EC           *
*     EI=imaginary part of EC      *
*     DWO=detuning angle           *
*     EANGLE=total phase angle     *
*     EINJ=injected signal         *
*****************************
      IMPLICIT REAL(B-H, O-S)
      DIMENSION DW(0:51), EC(0:51), EI(0:51), RE(0:51)
      DIMENSION  EANGLE(0:51), GAIN(0:51), EC2(0:16), DET(0:16)
      DIMENSION RTT(0:16), DT(0:16)
      PARAMETOR PI=4.0*ATAN(1.0)
-----------------------------------------------------------------------------

20    FORMAT (' INPUT Gain AND Gain without Losses ')
      PRINT 20
      ACCEPT *, GAINO, GNL

      NRTT=0

C   Initialize for system in steady state before Q-switch occurs

      DO 50 I=0,15
      EINJ=1.0
      DWO=I*0.2

C   A more accurate initialization of EI, and RE uses Eq. 4 from Sec. II.

      EI(0)=0
      RE(0)=EINJ
      EC(0)=EINJ
      EANGLE(0)=0
      DW(0)=DWO

C   Circulate within the cavity until the circulating signal reaches a predetermined value.
```

```
      DO 100 J=1,45

C    Set cavity gain and injected signal durring Q-switch turn on (case of high contrast Q-
C       switch).

      IF (J.LE.16) THEN
         CLOSS=1000-(997.1655*SIN(.09817*J)**2)
         GAIN(J)=SQRT(GNL/CLOSS)
         EINJ=COS(.09817*J)**2
      ELSE
         GAIN(J)=GAINO
         EINJ=0.0
      END IF

C    Round trip change in circulating signal.

      RE(J)=EC(J-1)*GAIN(J)*COS(EANGLE(J-1)+DWO)+EINJ
      EI(J)=EC(J-1)*GAIN(J)*SIN(EANGLE(J-1)+DWO)

      IF( EI(J).GE.0.0) THEN
         EANGLE(J)=ATAN2(EI(J),RE(J))
      END IF

      IF( EI(J).LT.0.0) THEN
         EANGLE(J)=2.0*PI+ATAN2(EI(J),RE(J))
      END IF

      DW(J)=EANGLE(J-1)+DWO-EANGLE(J)

      IF(EANGLE(J-1)+DWO.GT.6.28319) THEN
         IF(EANGLE(J).LT.3.14159) THEN
            DW(J)=EANGLE(J-1)+DWO-(2*PI+EANGLE(J))
         END IF
      END IF

         ANUMBER=J
         EC(J)=SQRT(RE(J)*RE(J)+EI(J)*EI(J))

C       Branch out if circulating singal exceeds preset limit.

         IF (EC(J).GE.1500000.0) GOTO 1000
100      CONTINUE

C       Determine round trip time with linear fit.

1000    DET(I)=DWO
         RUPPER=LOG(1500000.0)-LOG(EC(ANUMBER-1))
         RLOWER=LOG(EC(ANUMBER))-LOG(EC(ANUMBER-1))
         RTT(I)=ANUMBER+RUPPER/RLOWER
C
50      CONTINUE
C
         DO 200 I=0,15
```

```
           TYPE *, DET(I)
200     CONTINUE

        DO 300 I=0,15
        TYPE *, RTT(I)
300     CONTINUE
        STOP
        END
```

References

1. Y.K. Park, "Frequency and Mode Control of Q-Switched Lasers," Ph.D. dissertation, Ginzton Laboratory of Physics, Stanford Univ., Stanford, CA, 1981.

2. Y. K. Park, G. Giuliani, and R. L. Byer, "Stable single axial mode operation of an unstable resonator Nd:YAG oscillator by injection locking," *Opt. Lett.*, vol. 5, pp. 96-98, Mar. 1980.

3. Bingkun Zhou, Thomas J. Kane, George J. Dixon, and Robert L. Byer, "Efficient, frequency-stable laser-diode-pumped Nd:YAG laser," *Opt. Lett.*, vol. 10, pp. 62-64, Feb. 1985.

4. D. L. Sipes, "Highly efficient neodymium: yttrium aluminum garnet laser end pumped by a semiconductor laser array," *Appl. Phys. Lett.*, vol. 47, pp. 74-76,1985.

5. Adelbert Owyoung, G. R. Hadley, and Peter Esherick, "Gain switching of a monolithic single-frequency laser-diode-excited Nd:YAG laser," *Opt. Lett.*, vol. 10, pp.484-486, Oct. 1985.

6. T. Y. Fan, G. J. Dixon, and Robert L. Byer, "Efficient GaAlAs diode-laser-pumped operation of Nd:YLF at 1.047 μm with intracavity doubling to 523.6nm," *Opt. Lett.*, vol. 11, pp. 204-206, April 1986.

7. Randal L. Schmitt and Larry A. Rahn, "Diode-laser-pumped Nd:YAG laser injection seeding system," *Appl. Opt.*, vol. 25, pp.629-633, Mar. 1986.

8. Y.K. Park, G. Giuliani, and Robert L. Byer, "Single Axial Mode Operation of a Q-Switched Nd:YAG Oscillator by Injection Seeding," *IEEE J. Quant. Electornics*, vol. QE-20, pp. 117-125, Feb. 1984.

9. Jean-Louis Lechambre, Pierre Lavigne, Gabriel Otis, and Michel Noel, "Injection Locking and Mode Selection in TEA-CO_2 Laser Oscillators," *IEEE J. Quant. Electronics*, vol. QE-12, pp.756-764, Dec. 1976.

10. Anthony E. Siegman, *Lasers* (Mill Valley, Ca.: University Science Books, 1986), Chap. 29.

11. Ibid, p. 552.

12.   Joseph T. Verdeyen, *Laser Electronics* (Englewood Cliffs, N.J.: Prentice-Hall Inc.,1981).

13.   Larry A. Rahn, "Feedback stabilization of an injection-seeded Nd:YAG laser," *Appl. Opt.*, vol. 24, pp. 940-942, 1985.

14.   Richard E. Teets, "Feedback to Maintain Injection Locking of Nd:YAG Lasers," *IEEE J. Quant. Electronics*, vol. QE-20, pp. 326-328, 1984.

15.   Peter Esherick and Adelbert Owyoung, "Polarization feedback stabilization of an injection-seeded Nd:YAG laser for spectroscopic applications," *J. Opt. Soc. Am. B*, vol. 4, pp. 41-47, 1987.

16.   T. W. Hansch and B. Couillaud, "Laser Frequency Stabilization by Polarization Spectroscopy of a Reflecting Reference Cavity," *Optics Comm.*, vol. 35, pp. 441-444, 1980.

17.   Siegman, loc. cit., p. 422.